Supplementary Material for

Designer membraneless organelles enable codon reassignment of selected mRNAs in eukaryotes

Christopher D. Reinkemeier, Gemma Estrada Girona, Edward A. Lemke*
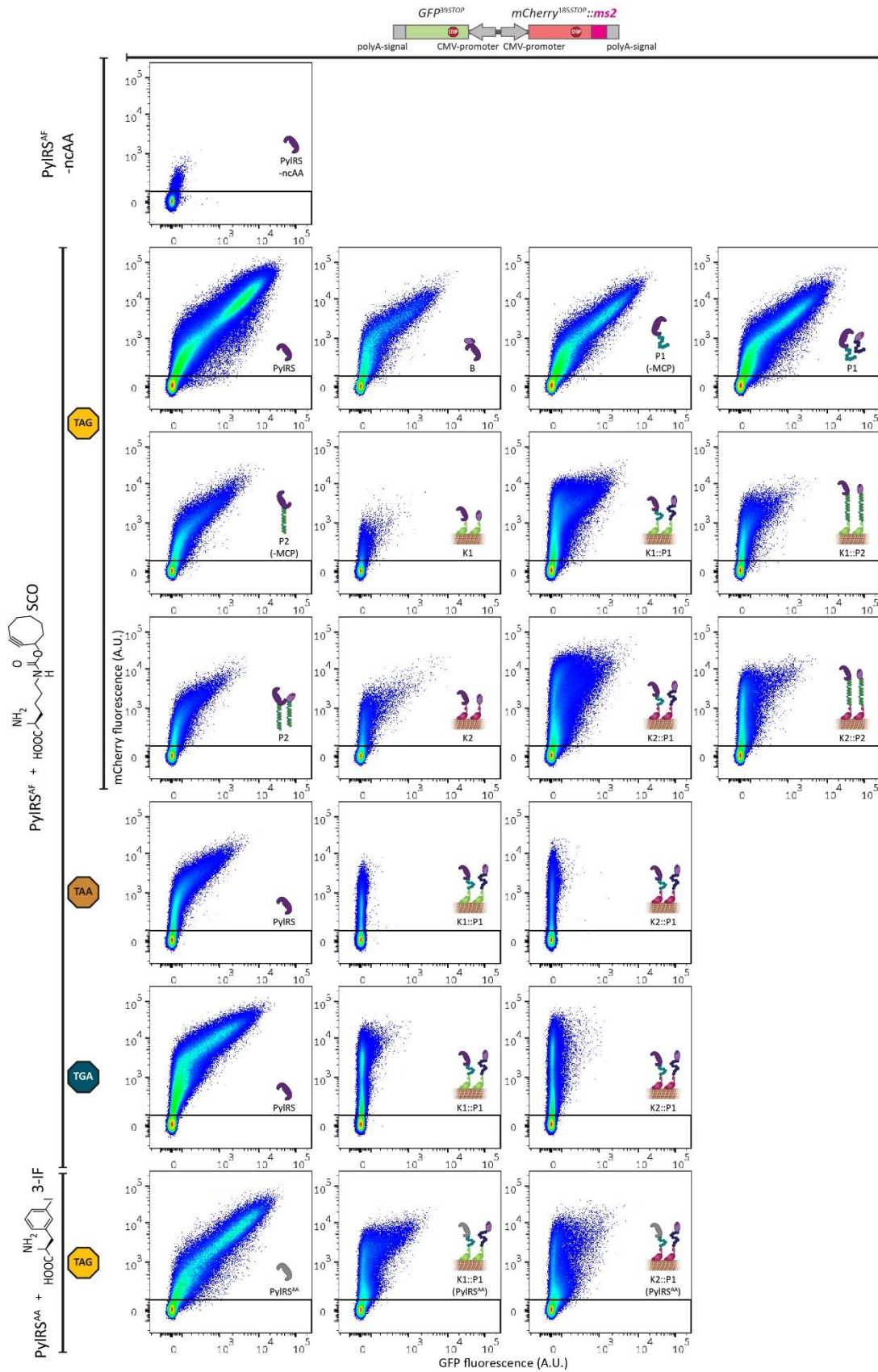
*Corresponding author. Email: edlemke@uni-mainz.de

This PDF file includes:

Figs. S1 to S9

Other Supplementary Material for this manuscript includes the following:
(available at www.sciencemag.org/content/363/6434/eaaw2644/suppl/DC1)

Movie S1

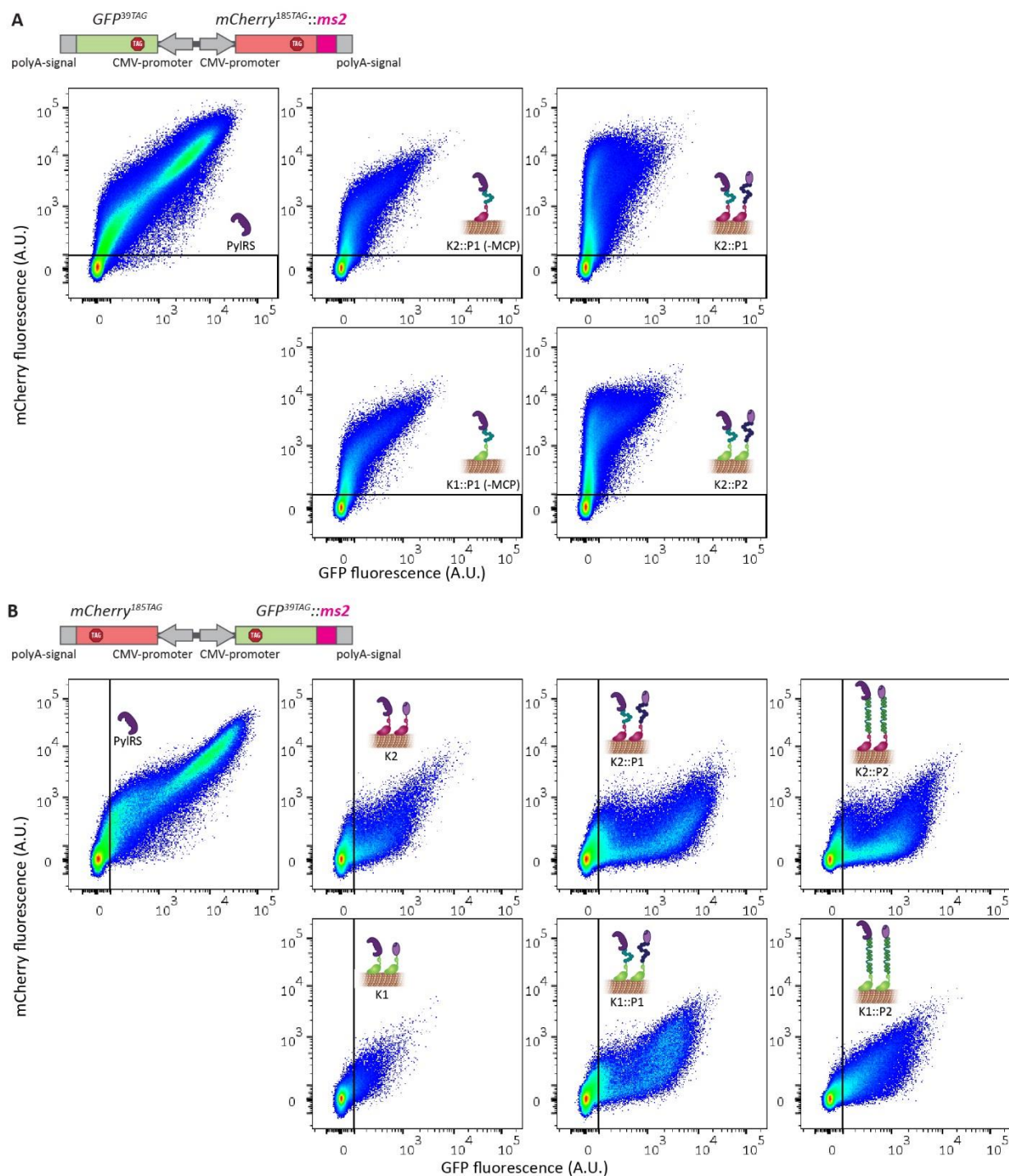**Fig. S1. FFC dot plot data corresponding to the bar graph in Fig. 2.**

FFC of HEK293T cells expressing the dual-color reporter (mCherry[185TAG] tagged with ms2 loops and GFP[39TAG]), tRNA[Pyl] and the indicated system. Plots show the sum of at least three independent experiments and the axes represent fluorescence intensities in arbitrary units. For transfections with PylRS[Y306A, Y384F] (PylRS[AF]) encoding constructs, the ncAA SCO (cyclooctynyl lysine) was added at a concentration of 250 µM, for PylRS[N346A, C348A] (PylRS[AA]) 3-iodophenylalanine was added at a concentration of 1 mM (structures indicate used ncAAs). In addition also Opal (TGA) and Ochre (TAA) stop codons were tested by performing experiments with GFP[39TGA]•mCherry[185TGA]::ms2 or GFP[39TAA]•mCherry[185TAA]::ms2 respectively (tRNA[Pyl] in these cases with the corresponding anticodons UCA or UUA). In the absence of ncAA, only very low background expression of mCherry and GFP is detected (for this minor background population, the efficiency was typically lower than 3% and the selectivity < 1.7 fold). In row 2 and 3 also data sets are show that did not contain MCP (corresponding to bar graph in maintext Fig. 2). Those serve as a negative control to validate that any observed selectivity effect is dependent on the interaction of MCP with ms2.
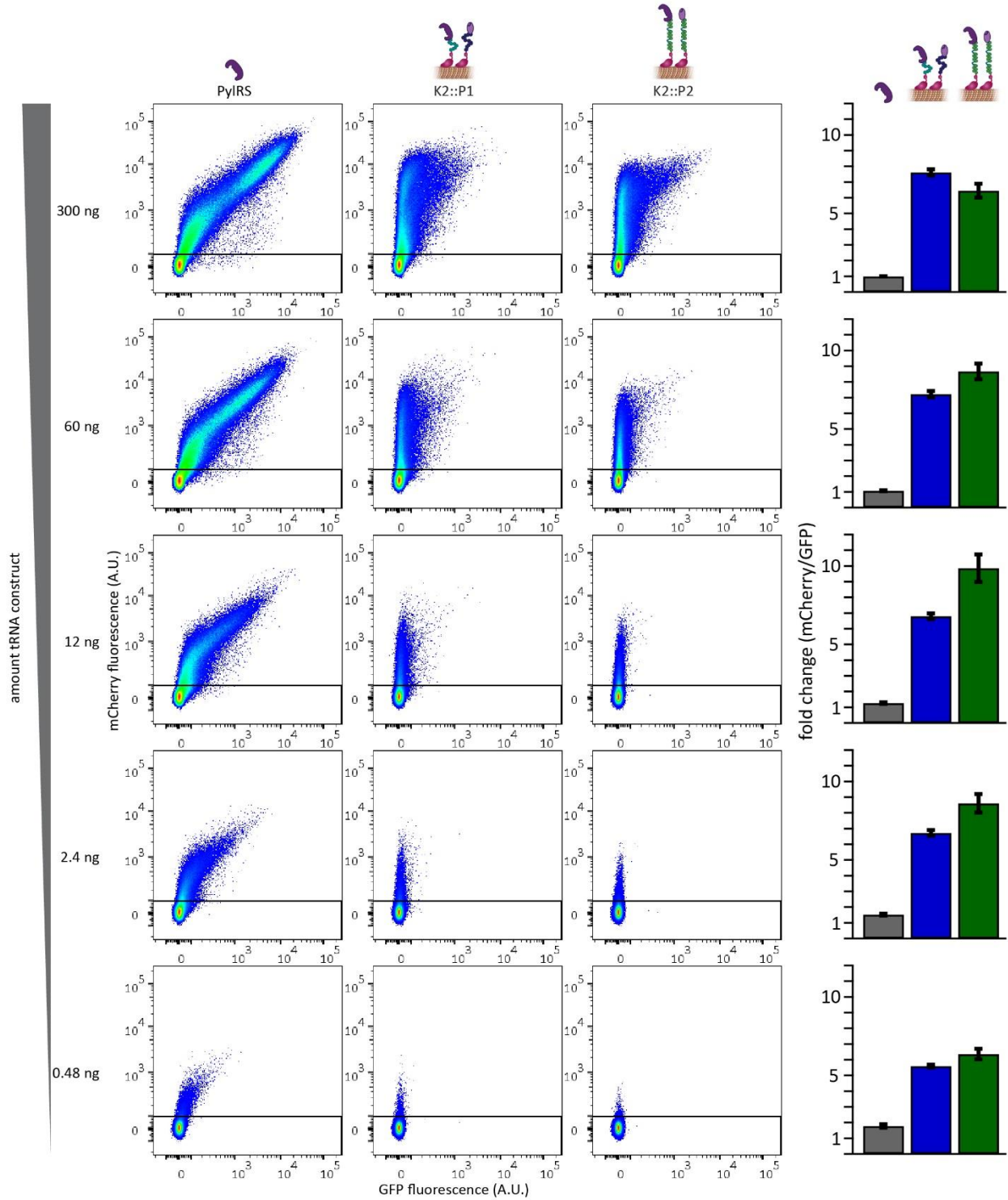
Fig. S2. The OT organelles function across a large dynamic working range of Amber suppression efficiency.

The concentration of tRNA^{Pyl} is known to be very important for Amber suppression *(21)*. Here we titrated the amount of *tRNA^{Pyl}* (ng of plasmid DNA given) to determine that the observed OT selectivity effect is robust across a large concentration and efficiency range of

Amber suppression. Shown are the corresponding FFC data as well as the bar plot analysis for the tested cytoplasmic PylRS (grey bar), the OT$^{K2::P1}$ (blue bar) and the OT$^{K2::P2}$ (green bar) systems. To this end, HEK293T cells were transfected with the dual-color reporter (*mCherry^{185TAG}* tagged with ms2 loops and *GFP^{39TAG}*) and the indicated genetic code expansion system (300 ng each plasmid). Each system was tested against a range of tRNA^{Pyl} encoding constructs, while the total amount of DNA was adjusted to be kept constant by addition of a mock plasmid. All experiments were performed in the presence of SCO. Dot plots show the sum of three independent experiments and axes indicate fluorescence intensity in arbitrary units. The bar plots show the ratio of mCherry to GFP signal normalized to the transfection with the cytoplasmic *PylRS* and 300 ng *tRNA^{Pyl}* construct. Shown are mean values with SEM of three independent experiments. The selectivity gain of the two best performing OT organelles is robust (>5.5 and <10 fold) even across a three order of magnitude change in *tRNA^{Pyl}* amount.

Fig. S3. Additional validations that the OT organelle selectivity is dependent on the complex formation of MCP with ms2 loops.

(A) FFC analysis of HEK293T cells expressing the dual-color reporter (mCherry[185TAG] tagged with ms2 loops and GFP[39TAG]), tRNA[Pyl] and the indicated system. SCO was present in all cases. The result clearly shows that proper function (i.e. selective expression of only the ms2-
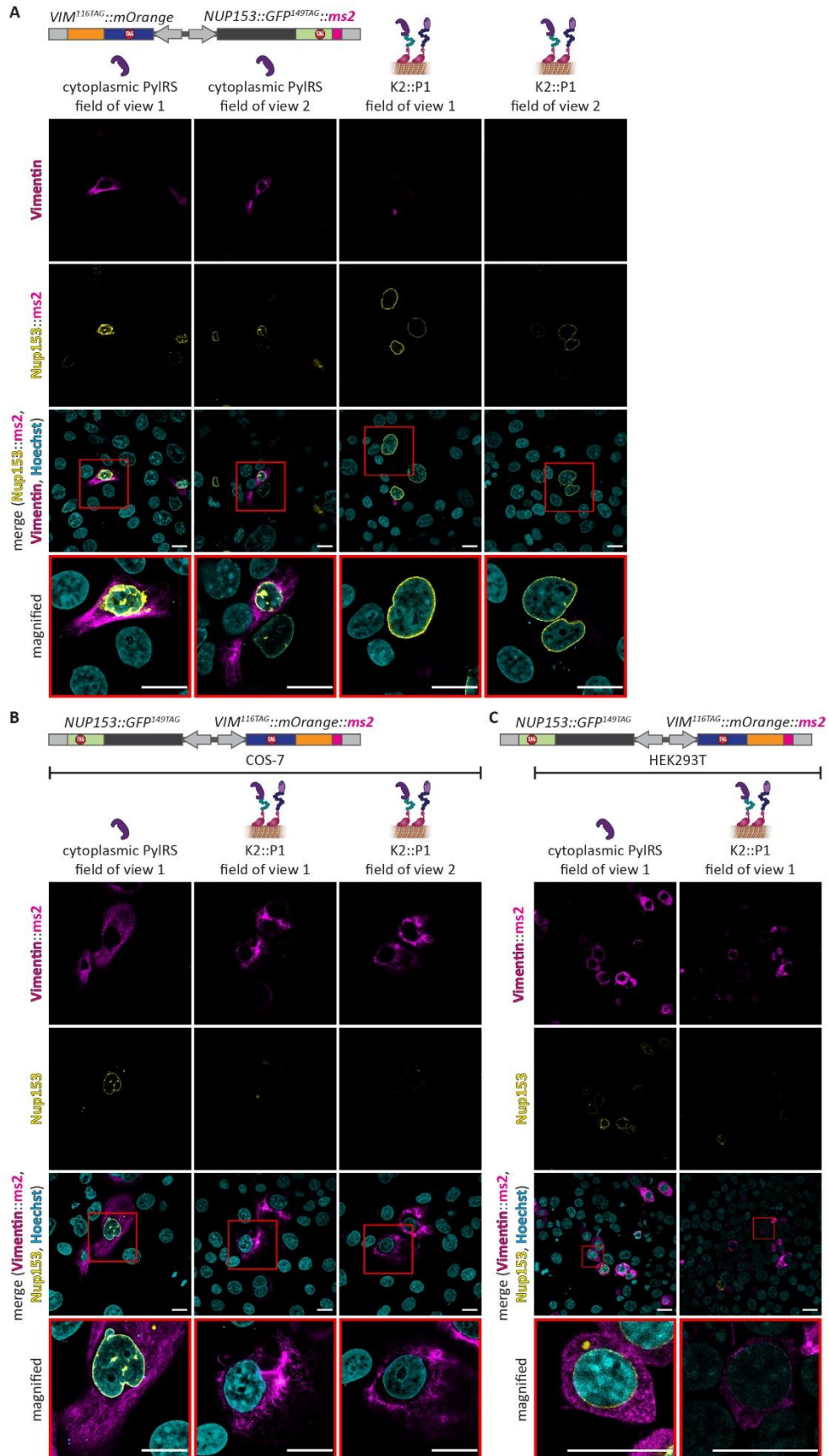
tagged mCherry^{185TAG}) of the OT organelles is dependent on the presence of MCP, since in the absence of MCP the FFC plots show a diagonal distribution similar to the cytoplasmic PylRS system. **(B)** FFC analysis of HEK293T cells expressing an inverted dual-color reporter (relative to main text, since here GFP^{39TAG} was tagged with ms2 loops instead of the mCherry^{185TAG}), tRNA^{Pyl} and the indicated system. In the presence of the OT organelles (**K2::P1**, **K2::P2**, **K1::P1** and **K1::P2**), now GFP is preferentially expressed. The result demonstrates that swapping the ms2-tag on the dual-color reporter swaps also the FFC signal. All FFC plots show the sum of at least three independent experiments, the axes represent fluorescence intensity in arbitrary units.
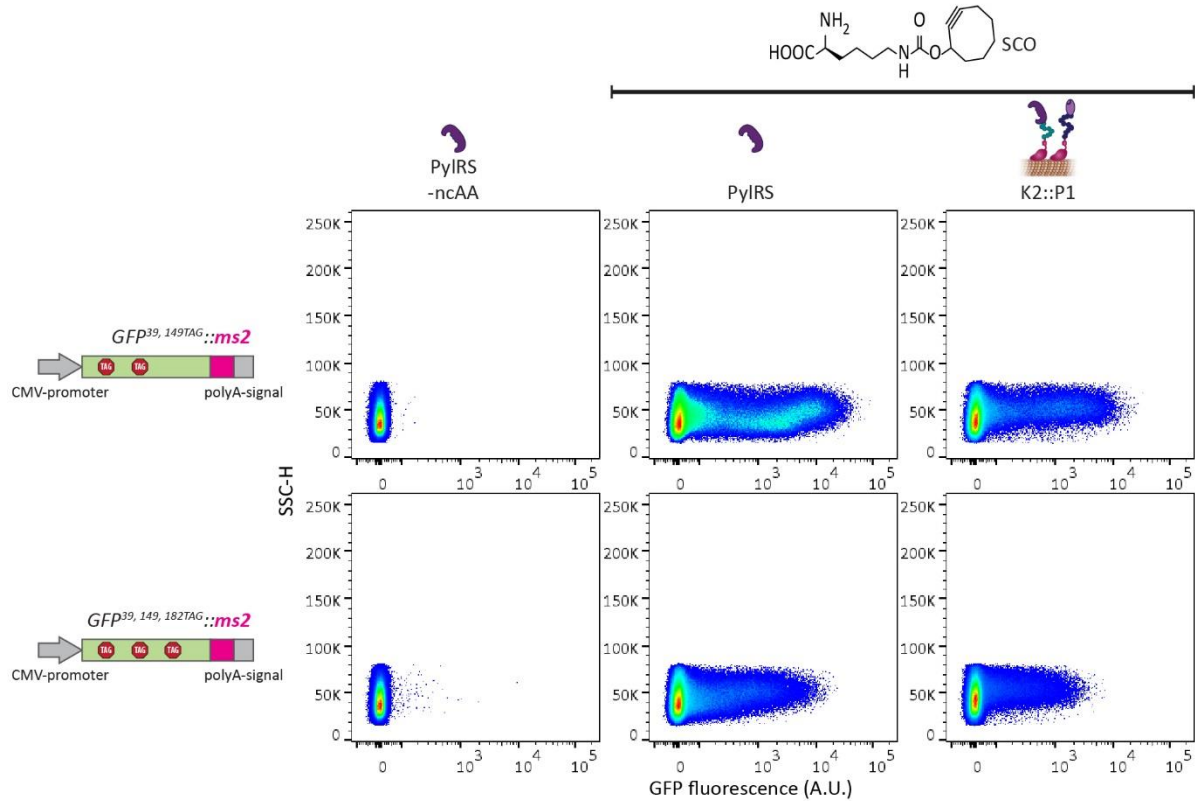
Fig. S4.The OT$^{K2::P1}$ organelle permits suppression of multiple Amber codons.

HEK293T cells were transfected with constructs encoding tRNA^{Pyl} together with either cytoplasmic PylRS or the OT$^{K2::P1}$ organelle and either a construct encoding the single color reporter GFP$^{39TAG, 149TAG}$::ms2 (dual Amber construct) or GFP$^{39TAG, 149TAG, 182TAG}$::ms2 (triple Amber construct) and analyzed via FFC. Plots show the sum of at least three independent experiments. Axes indicate side scatter height (SSC-H) vs GFP fluorescence intensity in arbitrary units. The data clearly show that like the cytoplasmic PylRS, the OT$^{K2::P1}$ organelle is capable of efficiently suppressing multiple Amber codons in one construct (~ 47% for dual Amber and ~ 53% for triple Amber relative to the corresponding cytoplasmic PylRS system for all cells with GFP fluorescence A.U. units >10^2).

A

VIM^{116TAG}::mOrange   *NUP153::GFP^{149TAG}::ms2*

cytoplasmic PylRS
field of view 1

cytoplasmic PylRS
field of view 2

K2::P1
field of view 1

K2::P1
field of view 2

Vimentin

Nup153::ms2

merge (Nup153::ms2, Vimentin, Hoechst)

magnified

B

NUP153::GFP^{149TAG}   *VIM^{116TAG}::mOrange::ms2*

COS-7

cytoplasmic PylRS
field of view 1

K2::P1
field of view 1

K2::P1
field of view 2

Vimentin::ms2

Nup153

merge (Vimentin::ms2, Nup153, Hoechst)

magnified

C

NUP153::GFP^{149TAG}   *VIM^{116TAG}::mOrange::ms2*

HEK293T

cytoplasmic PylRS
field of view 1

K2::P1
field of view 1

Vimentin::ms2

Nup153

merge (Vimentin::ms2, Nup153, Hoechst)

magnified

9

Fig. S5. The versatile OT$^{K2::P1}$ organelle enables selective and efficient orthogonal translation of a variety of proteins (this figure shows the complementary HEK293T or COS-7 experiments to maintext Fig. 3).

(**A-C**) Confocal images of cells transfected with constructs encoding PylRS or the OT$^{K2::P1}$ organelle for different protein pairs. SCO and tRNA^{Pyl} were present in all cases. (**A**) COS-7 cells were transfected with *NUP153::GFP^{149TAG}::ms2* and *VIM^{116TAG}::mOrange*. (**B,C**) *VIM^{116TAG}::mOrange::ms2* and *NUP153::GFP^{149TAG}* transfected in COS-7 cells ((**B**), analog to maintext Fig. 3B) and HEK293T cells (**C**). Top to bottom: Vimentin^{116TAG}::mOrange (magenta), Nup153::GFP^{149TAG} (yellow), overlay with Hoechst (cyan) and magnified images of representative cells (see red boxes; scale bars, 20 µm). The experiments clearly show for a variety of proteins and two different cell types, that in the presence of the OT$^{K2::P1}$ organelle, only the ms2 carrying mRNA is translated, while the cytoplasmic PylRS system always translates both.

	PyIRS (IF)	MCP (IF)	merge (MCP, PyIRS, NLS::GFP³⁹ᵀᴬᴳ::ms2)	magnified
PyIRS				
P1				
P2				
K1				
K2				
K1::P1				
K2::P1				
K1::P2				
K2::P2				

11
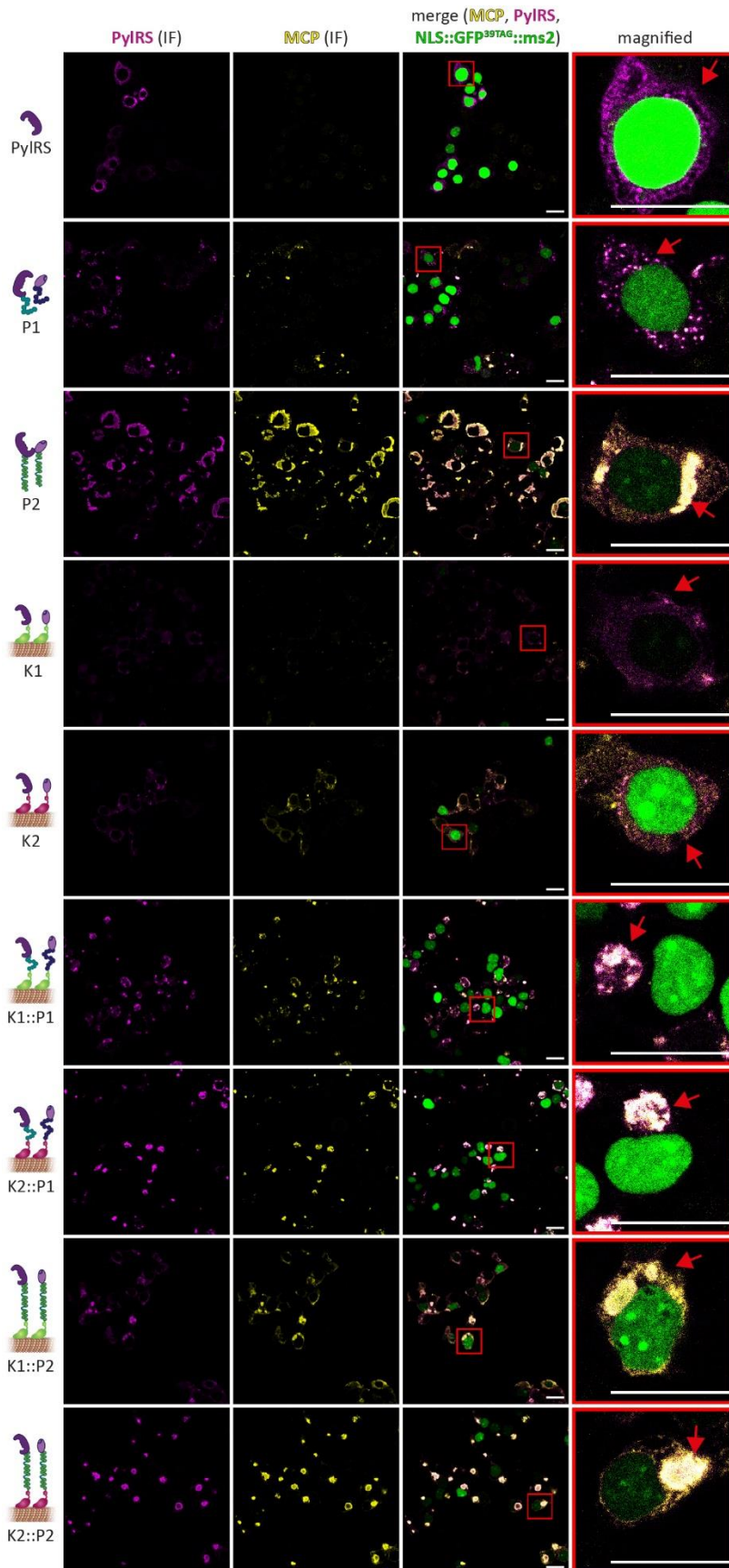
Fig. S6. Different dual imaging combinations to verify that assembler::MCP always colocalizes with assembler::PylRS.

(**A**) In maintext Fig. 4 we showed that tRNA^{Pyl} (visualized by FISH) and PylRS (visualized by IF) colocalize well. Complementary to this, here we show that also PylRS and MCP fused to the assemblers colocalize. IF of HEK293T cells expressing NLS::GFP^{39TAG}::ms2 with tRNA^{Pyl} and the indicated system. Note, that in general IF stainings appear crisper than FISH stainings. Left to right: PylRS (magenta), MCP (yellow), merge (NLS::GFP^{39TAG}::ms2 in green) and magnified image (see red box). NLS::GFP^{39TAG} yields nuclear fluorescence only if Amber suppression was successful, and helps here to identify cells in which transfection with all necessary plasmids occurred. All magnified zooms were centered on GFP positive cells. However, color settings were kept constant through this work for consistency and GFP expression differed between tested system (and cells), consistent with the observed Amber suppression efficiencies for the different systems, which in some cases were very low. Scale bars are 20 µm and in all magnified images red arrows point to representative structures as discussed in maintext Fig. 4.
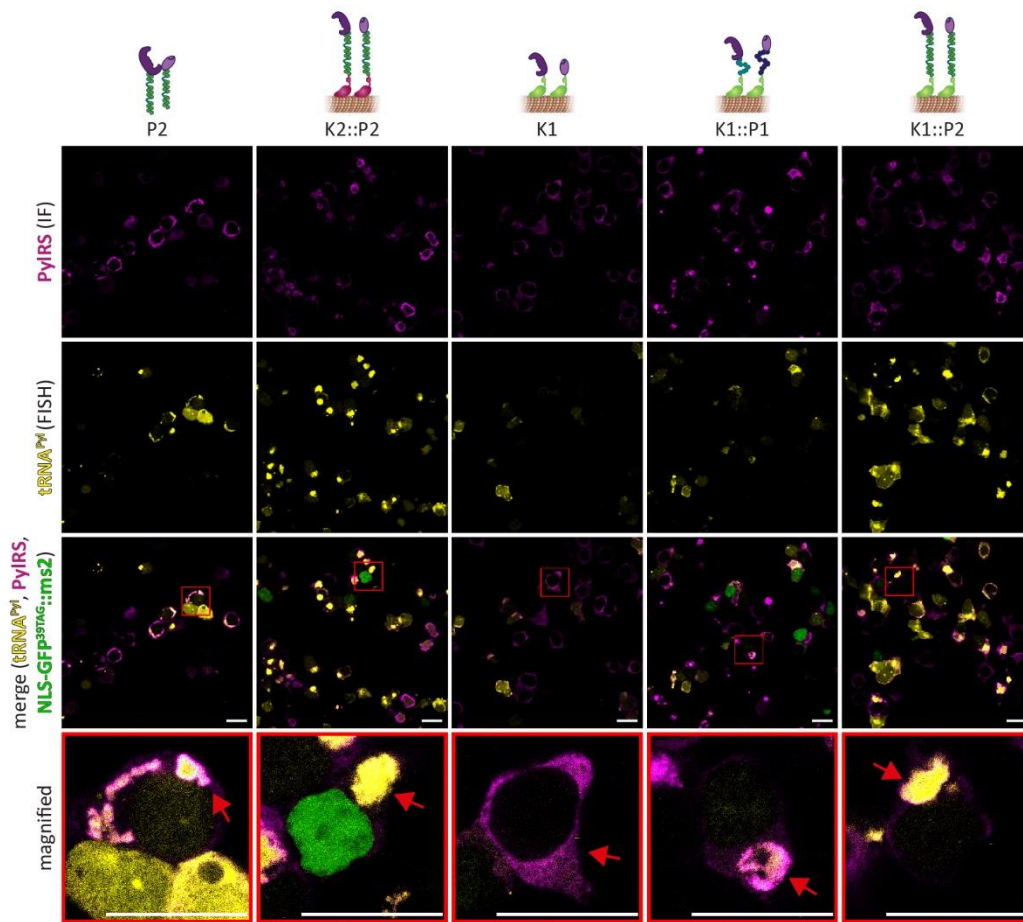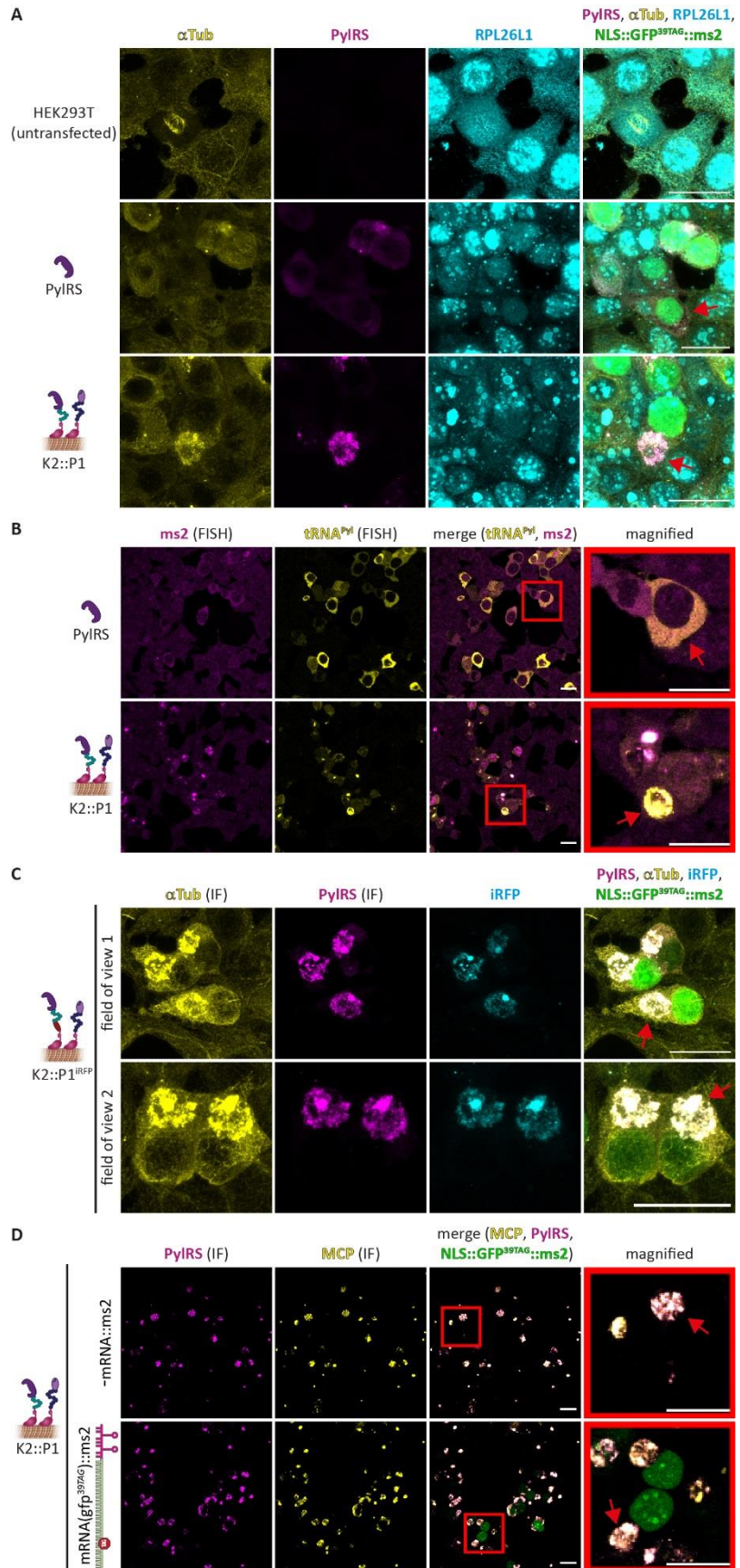
Fig. S7. PylRS and tRNA^{Pyl} colocalize for different KIF and SPD5 assembler systems (complementary to maintext Fig. 4).

In maintext Fig. 4 we showed colocalization of tRNA^{Pyl} and PylRS for assembler systems **P1**, **K2** and **K2::P1**. Here we show that they also colocalize for **P2**, **K2::P2**, **K1**, **K1::P1** and **K1::P2**. IF and FISH imaging of HEK293T cells expressing tRNA^{Pyl}, NLS::GFP^{39TAG}::ms2 and the indicated system. Top to bottom: IF against PylRS (magenta), FISH against tRNA^{Pyl} (yellow), merge (NLS::GFP^{39TAG}::ms2 in green) and magnified images of representative cells (see red boxes, red arrows highlight representative structures as discussed in maintext Fig. 4, scale bars, 20 µm). All magnified zooms were centered on GFP positive cells. However, color settings were kept constant through this work for consistency and GFP expression differed between tested system (and cells), consistent with the observed Amber suppression efficiencies for the different systems, which in some cases were very low.

The colocalization analysis is in line with the working hypothesis that selectivity is highly dependent on the partition coefficient of tRNA^{Pyl} into the OT organelle. For the three systems where droplet appearance is clearly visible (**P1**, **P2**, **K2::P1**), a qualitative analysis of the relative intensity ratio (IR) of droplets vs. cytoplasm (here used as a qualitative proxy for the partition coefficient; IR = intensity of droplets/intensity in cytoplasm) correlates well with the observed selectivity yielding IR(**K2::P1**) >> IR(**P2**) ~ IR(**P1**). However, despite the general challenges of

quantitative imaging in cells to establish exact concentrations of proteins *(29)*, the fact that we compare droplets of very different size make absolute quantitation very difficult. In addition, all those system show some selectivity, indicative of a depletion of tRNA^{Pyl} from the cytoplasm to varying degrees. The remaining tRNA^{Pyl} levels in the cytoplasm are hardly distinguishable from background fluorescence, so that we found any form of quantitation to be highly dependent on set parameters (threshold, background correction etc.). The trend, however was robust IR(**K2::P1**) >> IR(**P2**) ~ IR(**P1**). We suggest that in the future quantitative technologies such as in cell fluorescence correlation spectroscopy or quantitative super resolution microscopy could be used to measure the concentration of compounds in the droplet directly.

A

	αTub	PylRS	RPL26L1	PylRS, αTub, RPL26L1, NLS::GFP³⁹ᵀᴬᴳ::ms2
HEK293T (untransfected)				
PylRS				
K2::P1				

B

	ms2 (FISH)	tRNAᴾʸˡ (FISH)	merge (tRNAᴾʸˡ, ms2)	magnified
PylRS				
K2::P1				

C

	αTub (IF)	PylRS (IF)	iRFP	PylRS, αTub, iRFP, NLS::GFP³⁹ᵀᴬᴳ::ms2
K2::P1^iRFP field of view 1				
field of view 2				

D

	PylRS (IF)	MCP (IF)	merge (MCP, PylRS, NLS::GFP³⁹ᵀᴬᴳ::ms2)	magnified
K2::P1 -mRNA::ms2				
mRNA(gfp³⁹ᵀᴬᴳ)::ms2				

15

Fig. S8. RPL26L1, α-Tubulin and mRNA::ms2 colocalize with OT$^{K2::P1}$ organelle, its structure is not changed by the presence of mRNA::ms2.

(**A**) Maximum intensity Z-projection of IF of either untransfected HEK293T cells or HEK293T cells transfected with tRNA^{Pyl}, NLS::GFP^{39TAG}::ms2 and PylRS or OT$^{K2::P1}$ encoding constructs. Left to right: α-Tubulin (yellow), PylRS (magenta), RPL26L1 (cyan) and merge (NLS::GFP^{39TAG}::ms2 in green, scale bars 20 µm). This image series shows that microtubules and ribosomes colocalize in the OT$^{K2::P1}$ organelle.

(**B**) In Fig. 4, S6 and S7 we have shown that tRNA^{Pyl}, PylRS, MCP colocalize to OT organelles. Here we use FISH against mRNA::ms2 to visualize that also our targeted mRNA was recruited to the OT$^{K2::P1}$ organelle. FISH was performed in HEK293T cells expressing the dual-color reporter mRNAs (GFP^{39TAG}, mCherry^{185TAG}::ms2) as well as tRNA^{Pyl} and PylRS or the OT$^{K2::P1}$ organelle (here, no ncAA was present to avoid formation of fluorescent proteins interfering with image analysis). Left to right ms2 (magenta), tRNA^{Pyl} (yellow), merge and magnified images (see red box).

(**C**) Maximum intensity Z-projection of IF of HEK293T cells expressing with tRNA^{Pyl}, NLS::GFP^{39TAG}::ms2 and OT$^{K2::P1}$, in which KIF16B::FUS::PylRS is genetically tagged with iRFP. Left to right: α-Tubulin (yellow), PylRS (magenta), iRFP (cyan) and merge (NLS::GFP^{39TAG}::ms2 in green). This image series shows that the hollow appearance of the OT$^{K2::P1}$ organelle cannot be attributed to a staining artefact. We believe that the hollow appearance is rather linked to scaffolding to the Tubulin network, but not necessarily of functional relevance.

(**D**) IF of HEK293T cells transfected with constructs encoding tRNA^{Pyl}, OT$^{K2::P1}$ and either a mock plasmid or a plasmid encoding NLS::GFP^{39TAG}::ms2. Left to right: PylRS (magenta), MCP (yellow), merge (NLS::GFP^{39TAG}::ms2 in green) and magnified image (see red box). This image series shows that in OT$^{K2::P1}$ droplet-like appearance and colocalization of MCP and PylRS was detectable in cells expressing mRNA::ms2 and in cells without, indicating, that droplet formation did not depend on RNA recruitment.

(**A-D**) All scale bars are 20 µm and red arrows point to representative structures.
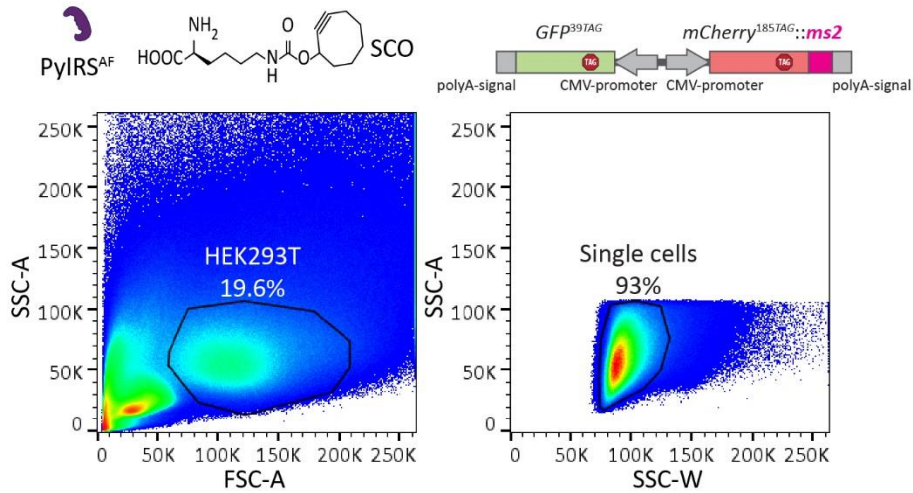
Fig. S9. Single HEK293T cells were sequentially identified based on scatter values.

As a representative example HEK293T cells expressing PylRS, tRNA^{Pyl} and the dual-color reporter (mCherry^{185TAG}::ms2 and GFP^{39TAG}) are shown (SCO was present in this experiment). Cells were first gated by cell type using forward scatter area (FSC-A) and side scatter area (SSC-A) parameters. Subsequently, single cells were identified based on SSC-A and side scatter width (SSC-W). Percentage next to gate name is based on the parent population (all data for SSC-A vs. FSC-A, HEK293T for SSC-A vs SSC-W). Cells passing the first gate (left panel) are further gated in the second (right) panel. All FFC data shown in this study were subjected to this analysis.

Movie 1: Complementary to maintext Fig. 4C here we show a movie of the 3D reconstruction.

3D reconstructions of IF images corresponding to those in maintext Fig. 4B,C. NLS::GFP^{39TAG}::ms2 (green), IF against RPL26L1 (cyan) and IF against PylRS (magenta). RPL26L1 staining inside the OT organelle demonstrates recruitment of ribosomes.

References and Notes

1. C. C. Liu, P. G. Schultz, Adding new chemistries to the genetic code. *Annu. Rev. Biochem.* **79**, 413–444 (2010). doi:10.1146/annurev.biochem.052308.105824 Medline

2. E. A. Lemke, The exploding genetic code. *ChemBioChem* **15**, 1691–1694 (2014). doi:10.1002/cbic.201402362 Medline

3. J. W. Chin, Expanding and reprogramming the genetic code. *Nature* **550**, 53–60 (2017). doi:10.1038/nature24031 Medline

4. H. Neumann, K. Wang, L. Davis, M. Garcia-Alai, J. W. Chin, Encoding multiple unnatural amino acids via evolution of a quadruplet-decoding ribosome. *Nature* **464**, 441–444 (2010). doi:10.1038/nature08817 Medline

5. C. Orelle, E. D. Carlson, T. Szal, T. Florin, M. C. Jewett, A. S. Mankin, Protein synthesis by ribosomes with tethered subunits. *Nature* **524**, 119–124 (2015). doi:10.1038/nature14862 Medline

6. S. D. Fried, W. H. Schmied, C. Uttamapinant, J. W. Chin, Ribosome Subunit Stapling for Orthogonal Translation in *E. coli*. *Angew. Chem.* **127**, 12982–12985 (2015). doi:10.1002/anie.201506311 Medline

7. F. J. Isaacs, P. A. Carr, H. H. Wang, M. J. Lajoie, B. Sterling, L. Kraal, A. C. Tolonen, T. A. Gianoulis, D. B. Goodman, N. B. Reppas, C. J. Emig, D. Bang, S. J. Hwang, M. C. Jewett, J. M. Jacobson, G. M. Church, Precise manipulation of chromosomes in vivo enables genome-wide codon replacement. *Science* **333**, 348–353 (2011). doi:10.1126/science.1205822 Medline

8. M. J. Lajoie, A. J. Rovner, D. B. Goodman, H.-R. Aerni, A. D. Haimovich, G. Kuznetsov, J. A. Mercer, H. H. Wang, P. A. Carr, J. A. Mosberg, N. Rohland, P. G. Schultz, J. M. Jacobson, J. Rinehart, G. M. Church, F. J. Isaacs, Genomically recoded organisms expand biological functions. *Science* **342**, 357–360 (2013). doi:10.1126/science.1241459 Medline

9. N. Ostrov, M. Landon, M. Guell, G. Kuznetsov, J. Teramoto, N. Cervantes, M. Zhou, K. Singh, M. G. Napolitano, M. Moosburner, E. Shrock, B. W. Pruitt, N. Conway, D. B. Goodman, C. L. Gardner, G. Tyree, A. Gonzales, B. L. Wanner, J. E. Norville, M. J. Lajoie, G. M. Church, Design, synthesis, and testing toward a 57-codon genome. *Science* **353**, 819–822 (2016). doi:10.1126/science.aaf3639 Medline

10. K. Wang, J. Fredens, S. F. Brunner, S. H. Kim, T. Chia, J. W. Chin, Defining synonymous codon compression schemes by genome recoding. *Nature* **539**, 59–64 (2016). doi:10.1038/nature20124 Medline

11. Y. Zhang, J. L. Ptacin, E. C. Fischer, H. R. Aerni, C. E. Caffaro, K. San Jose, A. W. Feldman, C. R. Turner, F. E. Romesberg, A semi-synthetic organism that stores and retrieves increased genetic information. *Nature* **551**, 644–647 (2017). doi:10.1038/nature24659 Medline

12. D. B. Thompson, S. Aboulhouda, E. Hysolli, C. J. Smith, S. Wang, O. Castanon, G. M. Church, The future of multiplexed eukaryotic genome engineering. *ACS Chem. Biol.* **13**, 313–325 (2018). doi:10.1021/acschembio.7b00842 Medline

13. C. P. Brangwynne, C. R. Eckmann, D. S. Courson, A. Rybarska, C. Hoege, J. Gharakhani, F. Jülicher, A. A. Hyman, Germline P granules are liquid droplets that localize by controlled dissolution/condensation. *Science* **324**, 1729–1732 (2009). doi:10.1126/science.1172046 Medline

14. P. Li, S. Banjade, H.-C. Cheng, S. Kim, B. Chen, L. Guo, M. Llaguno, J. V. Hollingsworth, D. S. King, S. F. Banani, P. S. Russo, Q.-X. Jiang, B. T. Nixon, M. K. Rosen, Phase transitions in the assembly of multivalent signalling proteins. *Nature* **483**, 336–340 (2012). doi:10.1038/nature10879 Medline

15. A. A. Hyman, C. A. Weber, F. Jülicher, Liquid-liquid phase separation in biology. *Annu. Rev. Cell Dev. Biol.* **30**, 39–58 (2014). doi:10.1146/annurev-cellbio-100913-013325 Medline

16. E. Bertrand, P. Chartrand, M. Schaefer, S. M. Shenoy, R. H. Singer, R. M. Long, Localization of ASH1 mRNA particles in living yeast. *Mol. Cell* **2**, 437–445 (1998). [doi:10.1016/S1097-2765(00)80143-4](doi:10.1016/S1097-2765(00)80143-4) Medline

17. M. Altmeyer, K. J. Neelsen, F. Teloni, I. Pozdnyakova, S. Pellegrino, M. Grøfte, M.-B. D. Rask, W. Streicher, S. Jungmichel, M. L. Nielsen, J. Lukas, Liquid demixing of intrinsically disordered proteins is seeded by poly(ADP-ribose). *Nat. Commun.* **6**, 8088 (2015). doi:10.1038/ncomms9088 Medline

18. A. Patel, H. O. Lee, L. Jawerth, S. Maharana, M. Jahnel, M. Y. Hein, S. Stoynov, J. Mahamid, S. Saha, T. M. Franzmann, A. Pozniakovski, I. Poser, N. Maghelli, L. A. Royer, M. Weigert, E. W. Myers, S. Grill, D. Drechsel, A. A. Hyman, S. Alberti, A liquid-to-solid phase transition of the ALS protein FUS accelerated by disease mutation. *Cell* **162**, 1066–1077 (2015). doi:10.1016/j.cell.2015.07.047 Medline

19. J. B. Woodruff, B. Ferreira Gomes, P. O. Widlund, J. Mahamid, A. Honigmann, A. A. Hyman, The centrosome is a selective condensate that nucleates microtubules by concentrating tubulin. *Cell* **169**, 1066–1077.e10 (2017). doi:10.1016/j.cell.2017.05.028 Medline

20. V. Soppina, S. R. Norris, A. S. Dizaji, M. Kortus, S. Veatch, M. Peckham, K. J. Verhey, Dimerization of mammalian kinesin-3 motors results in superprocessive motion. *Proc. Natl. Acad. Sci. U.S.A.* **111**, 5562–5567 (2014). doi:10.1073/pnas.1400759111 Medline

21. I. Nikić, T. Plass, O. Schraidt, J. Szymański, J. A. Briggs, C. Schultz, E. A. Lemke, Minimal tags for rapid dual-color live-cell labeling and super-resolution microscopy. *Angew. Chem.* **53**, 2245–2249 (2014). doi:10.1002/anie.201309847 Medline

22. T. Plass, S. Milles, C. Koehler, J. Szymański, R. Mueller, M. Wiessler, C. Schultz, E. A. Lemke, Amino acids for Diels-Alder reactions in living cells. *Angew. Chem.* **51**, 4166–4170 (2012). doi:10.1002/anie.201108231 Medline

23. T. Plass, S. Milles, C. Koehler, C. Schultz, E. A. Lemke, Genetically encoded copper-free click chemistry. *Angew. Chem.* **50**, 3878–3881 (2011). doi:10.1002/anie.201008178 Medline

24. H. Xiao, A. Chatterjee, S. H. Choi, K. M. Bajjuri, S. C. Sinha, P. G. Schultz, Genetic incorporation of multiple unnatural amino acids into proteins in mammalian cells. *Angew. Chem.* **52**, 14080–14083 (2013). doi:10.1002/anie.201308137 Medline

25. W. H. Schmied, S. J. Elsässer, C. Uttamapinant, J. W. Chin, Efficient multisite unnatural amino acid incorporation in mammalian cells via optimized pyrrolysyl tRNA synthetase/tRNA expression and engineered eRF1. *J. Am. Chem. Soc.* **136**, 15577–15583 (2014). doi:10.1021/ja5069728 Medline

26. Z. Zhang, H. Xu, L. Si, Y. Chen, B. Zhang, Y. Wang, Y. Wu, X. Zhou, L. Zhang, D. Zhou, Construction of an inducible stable cell line for efficient incorporation of unnatural amino acids in mammalian cells. *Biochem. Biophys. Res. Commun.* **489**, 490–496 (2017). doi:10.1016/j.bbrc.2017.05.178 Medline

27. Y. S. Wang, X. Fang, H.-Y. Chen, B. Wu, Z. U. Wang, C. Hilty, W. R. Liu, Genetic incorporation of twelve meta-substituted phenylalanine derivatives using a single pyrrolysyl-tRNA synthetase mutant. *ACS Chem. Biol.* **8**, 405–415 (2013). doi:10.1021/cb300512r Medline

28. I. Nikić, G. Estrada Girona, J. H. Kang, G. Paci, S. Mikhaleva, C. Koehler, N. V. Shymanska, C. Ventura Santos, D. Spitz, E. A. Lemke, Debugging eukaryotic genetic code expansion for site-specific click-PAINT super-resolution microscopy. *Angew. Chem.* **55**, 16172–16176 (2016). doi:10.1002/anie.201608284 Medline

29. S. F. Banani, A. M. Rice, W. B. Peeples, Y. Lin, S. Jain, R. Parker, M. K. Rosen, Compositional control of phase-separated cellular bodies. *Cell* **166**, 651–663 (2016). doi:10.1016/j.cell.2016.06.010 Medline

30. C. C. Liu, M. C. Jewett, J. W. Chin, C. A. Voigt, Toward an orthogonal central dogma. *Nat. Chem. Biol.* **14**, 103–106 (2018). doi:10.1038/nchembio.2554 Medline

31. J. R. Simon, N. J. Carroll, M. Rubinstein, A. Chilkoti, G. P. López, Programming molecular self-assembly of intrinsically disordered proteins containing sequences of low complexity. *Nat. Chem.* **9**, 509–515 (2017). doi:10.1038/nchem.2715 Medline

32. D. G. Gibson, L. Young, R.-Y. Chuang, J. C. Venter, C. A. Hutchison 3rd, H. O. Smith, Enzymatic assembly of DNA molecules up to several hundred kilobases. *Nat. Methods* **6**, 343–345 (2009). doi:10.1038/nmeth.1318 Medline

33. I. Nikić, J. H. Kang, G. E. Girona, I. V. Aramburu, E. A. Lemke, Labeling proteins on live mammalian cells using click chemistry. *Nat. Protoc.* **10**, 780–791 (2015). doi:10.1038/nprot.2015.045 Medline

34. J. B. Pierce, S. C. Chafe, M. B. Eswara, G. van der Merwe, D. Mangroo, Strategies for investigating nuclear-cytoplasmic tRNA dynamics in yeast and mammalian cells. *Methods Cell Biol.* **122**, 415–436 (2014). doi:10.1016/B978-0-12-417160-2.00019-9 Medline